NAVAL POSTGRADUATE SCHOOL

MONTEREY, CALIFORNIA

THESIS

BATHYMETRIC MAPPING WITH QUICKBIRD DATA

by

Martin Densham

September 2005

Thesis Advisor:	Philip A Durkee
Co-Advisor:	Edward B Thornton

Approved for public release; distribution is unlimited

THIS PAGE INTENTIONALLY LEFT BLANK

REPORT DOCUMENTATION PAGE			Form Approved OMB No. 0704-0188
Public reporting burden for this collection of information is estimated to average 1 hour per response, including the time for reviewing instruction, searching existing data sources, gathering and maintaining the data needed, and completing and reviewing the collection of information. Send comments regarding this burden estimate or any other aspect of this collection of information, including suggestions for reducing this burden, to Washington headquarters Services, Directorate for Information Operations and Reports, 1215 Jefferson Davis Highway, Suite 1204, Arlington, VA 22202-4302, and to the Office of Management and Budget, Paperwork Reduction Project (0704-0188) Washington DC 20503.			
1. AGENCY USE ONLY ***(Leave blank)***	**2. REPORT DATE** September 2005	**3. REPORT TYPE AND DATES COVERED** Master's Thesis	
4. TITLE AND SUBTITLE: Bathymetric Mapping with QuickBird Data.			**5. FUNDING NUMBERS**
6. AUTHOR(S) Martin P. J. Densham			
7. PERFORMING ORGANIZATION NAME(S) AND ADDRESS(ES) Naval Postgraduate School Monterey, CA 93943-5000			**8. PERFORMING ORGANIZATION REPORT NUMBER**
9. SPONSORING /MONITORING AGENCY NAME(S) AND ADDRESS(ES) N/A			**10. SPONSORING/MONITORING AGENCY REPORT NUMBER**
11. SUPPLEMENTARY NOTES The views expressed in this thesis are those of the author and do not reflect the official policy or position of the Department of Defense or the U.S. Government.			
12a. DISTRIBUTION / AVAILABILITY STATEMENT Approved for public release; distribution is unlimited.			**12b. DISTRIBUTION CODE**

13. ABSTRACT (maximum 200 words)

Two algorithms are used to determine bathymetry in the littoral region using QuickBird multi-spectral satellite observations. The algorithms determine water-leaving radiance and convert this to water depth values. The first algorithm uses a ratio of two wavebands and the second uses the sum of several wavebands. Relative bathymetric errors are determined for the clear water of Looe Key (USA) and the turbid water of Plymouth Sound (UK). Bathymetric measurements from LIDAR and chart data are compared to derived depths to assess their accuracies. An amended version of the ratio method is proposed for use in turbid water to improve accuracy. The results show that the standard ratio and turbidity algorithms have a relative error of 11.7% and 16.5% respectively in clear water. In turbid water the average error of the turbidity algorithm is 11.6% and the amended ratio algorithm average error is 13%.

14. SUBJECT TERMS Aerosol Optical Depth, AOD, Bathymetry, ENVI, HYDROLIGHT, LIDAR, QuickBird, Ratio Algorithm, Stratified Genetic Algorithm.			**15. NUMBER OF PAGES** 62
			16. PRICE CODE
17. SECURITY CLASSIFICATION OF REPORT Unclassified	**18. SECURITY CLASSIFICATION OF THIS PAGE** Unclassified	**19. SECURITY CLASSIFICATION OF ABSTRACT** Unclassified	**20. LIMITATION OF ABSTRACT** UL

NSN 7540-01-280-5500 Standard Form 298 (Rev. 2-89)
Prescribed by ANSI Std. 239-18

THIS PAGE INTENTIONALLY LEFT BLANK

Approved for public release; distribution is unlimited

BATHYMETRIC MAPPING WITH QUICKBIRD DATA

Martin P. J. Densham
Lieutenant, Royal Navy
M.A., Cambridge University, 1994

Submitted in partial fulfillment of the
requirements for the degree of

MASTER OF SCIENCE IN PHYSICAL OCEANOGRAPHY

from the

NAVAL POSTGRADUATE SCHOOL
September 2005

Author: Martin P. J. Densham

Approved by: Philip A. Durkee
Thesis Advisor

Edward B. Thornton
Thesis Co-Advisor

Mary L. Batteen
Chairman, Department of Oceanography

THIS PAGE INTENTIONALLY LEFT BLANK

ABSTRACT

Two algorithms are used to determine bathymetry in the littoral region using QuickBird multi-spectral satellite observations. The algorithms determine water-leaving radiance and convert this to water depth values. The first algorithm uses a ratio of two wavebands and the second uses the sum of several wavebands. Relative bathymetric errors are determined for the clear water of Looe Key (USA) and the turbid water of Plymouth Sound (UK). Bathymetric measurements from LIDAR and chart data are compared to derived depths to assess their accuracies. An amended version of the ratio method is proposed for use in turbid water to improve accuracy. The results show that the standard ratio and turbidity algorithms have a relative error of 11.7% and 16.5% respectively in clear water. In turbid water the average error of the turbidity algorithm is 11.6% and the amended ratio algorithm average error is 13%.

THIS PAGE INTENTIONALLY LEFT BLANK

TABLE OF CONTENTS

LIST OF FIGURES

THIS PAGE INTENTIONALLY LEFT BLANK

LIST OF TABLES

THIS PAGE INTENTIONALLY LEFT BLANK

ACKNOWLEDGMENTS

I would like to thank my advisor, Dr. Philip A. Durkee, Chairman of the Department of Meteorology, and Dr. Ed Thornton, Distinguished Professor, my Co-Advisor, both of the Naval Postgraduate School, for their guidance and advice during the thesis process.

Many thanks go to LCDR Nick Vincent and Mr. Kurt Nielsen for their technical expertise and patience in assisting my research. Thanks also go to Mr. Graeme Potter who arranged the collection and transfer of data to the U.S. from the United Kingdom Hydrographic Office.

I would like to thank LT CDR Mike Cooper, LT Billy Roeting and Capt Matt Taylor for their help and humour during my time in the Remote Sensing Laboratory. Finally, many thanks go Greta and Scrub for making my time in America so enjoyable.

THIS PAGE INTENTIONALLY LEFT BLANK

I. INTRODUCTION

Remote sensing has become an increasingly important application for bathymetric mapping since its inception as a tool to determine water depth over twenty years ago. As a result of an increase in the availability of commercially provided high-resolution multi-spectral satellite imagery, such as Quick Bird, SPOT, IKONOS and Landsat, the accuracy of water depth analysis has improved accordingly (Stumpf et al, 2003). Given that bathymetry can be determined at substantially less cost and more expediently by remote sensing techniques than traditional hydrographic methods, an analysis of its accuracy in a range of environments is proposed to determine usability in differing operational environments.

Remote sensing data can potentially service a range of requirements including navigation data, updates to the Digital Bathymetric Data Base (DBDB), inputs to modeling algorithms for surf, current and acoustic predictions, mine detection, Beach Intelligence Survey Data and environmental monitoring. In order to achieve these requirements, a degree of accuracy must be achieved. Current accuracy comparisons with hydrographic data show mean errors in the range of 10-30% with a maximum effective depth ranging from 6-10.5m (Lafon et al, 2002, Tanis et al, 2002). The major source of error is the compounded attenuation by the atmosphere and water column on radiance reflected by the seabed and received by the satellite.

The basic premise behind water depth calculations is that the radiance received by the satellite is a function of five parameters: incoming solar radiation; attenuation of radiation into and out of the atmosphere; attenuation of radiation into and out of the water column; reflectance properties of the seabed and the depth of water. The depth of water can be resolved by finding values for the first four parameters (Lyzenga, 1981). Several techniques exist to achieve this, they fall into three main categories:

1) The first are linear methods that solve empirically for several variables, then use Beer's Law, which states that light decays exponentially with

depth in the water column (Lyzenga, 1981, 1985). A single waveband is used to determine water depth for each pixel.

2) The second are ratio methods, which use two or more wavebands to determine the depth of water based on the differing attenuation properties of the multiple wavelengths. Radiance values from these wavebands solve for depth through correlation with known ratios for a specific water column. These methods have fewer parameters to solve for and are less affected by changes in bottom reflectance as both wavelengths are affected similarly by bottom albedo (Stumpf et al, 2003).

3) The third type consists of variations on the linear method. The Stratified Genetic Algorithm uses a method that splits the water column into levels of differing attenuations (due to turbidity) and calculates a sum of ratios for several wavelengths (Gianinetto et al, 2003)

The potential for error exists because of the difficulty in accurately determining the optical properties of the atmosphere, ocean and seabed. Unfortunately model data must be used as there is little chance in an operational situation to take in situ measurements at the time of image capture. The objectives of this thesis are to compare each method's performance in a range of different environmental conditions and evaluate relative accuracies against hydrographic and Lidar survey data.

Chapter II provides a review of relevant atmosphere and ocean optical properties and the radiative transfer equation. Chapter III outlines the data used. Chapter IV discusses the applications and methods used to analyse the data. Chapter V presents the results and Chapter VI summarises the conclusions and recommendations.

II. BACKGROUND

Central to retrieving water depth information from remotely sensed radiance values are accurate corrections for attenuation and back-scattering within the atmosphere and water column. Radiative transfer theory relates the measured radiance at the sensor to the interaction between incoming solar radiation, atmospheric aerosols (Martin, 2004) and water column attenuation (Jupp, 1988). Corrections for the effects of the atmosphere and water column must be applied to the remotely sensed data to isolate the measured radiance as a function of water depth. The total radiation measured at the satellite is the product of incoming solar radiation, attenuation within the atmosphere and water column, atmospheric backscatter, water surface reflectance, substrata reflectance and water depth.

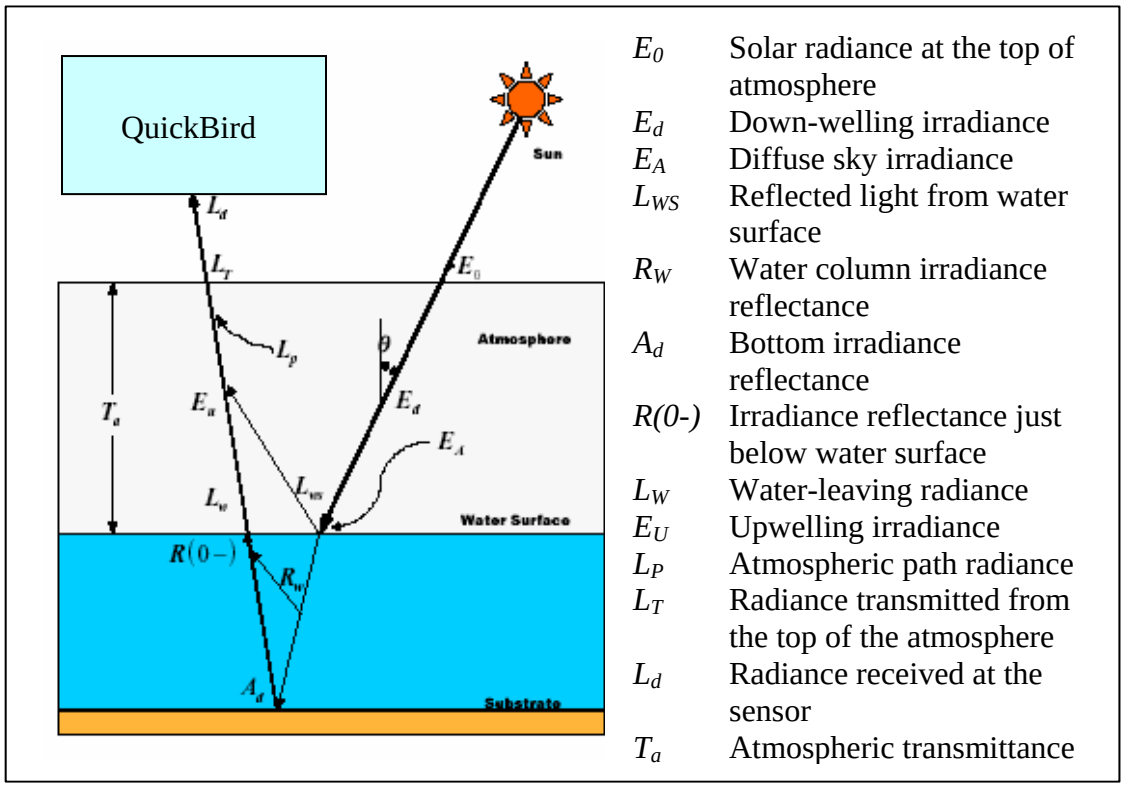

Figure 1. Factors that influence radiance reaching a sensor over a water mass. (After: Bierwirth et al,1992).

A. OPTICAL PROPERTIES OF THE ATMOSPHERE

Radiative transfer theory outlines four main sources of photons that contribute to the total radiance received by a sensor at the top of the atmosphere (Durkee et al, 1986):

$$L_t = L_r + L_a + \left(L_g + L_s\right)\tau_d \,, \qquad (2.1)$$

where L_t is the total radiance received by the sensor, L_r is the molecular Rayleigh scattering radiance, L_a is the aerosol scattering radiance, L_g is the radiance from surface glint, L_s is the surface radiance and τ_d is the transmittance of the of the direct path. Atmospheric scattering is calculated to separate the surface radiance from the total radiance. A surface reflectance algorithm is used to calculate the amount of reflection produced by surface glint (or specular reflection) and this value is then removed from the top of the atmosphere radiance. Model calculations are used to assess molecular Rayleigh scattering within different wavebands and the information incorporated into the NPS aerosol model. Using linearized single scatter theory (LSS), this model solves for overall atmospheric scattering radiance given as:

$$L_t\left(\lambda,\theta,\phi\right) = L_0\left(\lambda,\theta,\phi\right)e^{-\delta(\lambda)/\mu} + \frac{\omega_0\left(\lambda\right)p\left(\psi_s,\lambda\right)\delta\left(\lambda\right)L\left(\theta_0,\phi_0,\lambda\right)}{4\pi\mu}, \qquad (2.2)$$

where λ is wavelength, θ is the satellite zenith angle, φ is the satellite azimuth angle, L_0 is surface radiance, $e^{-\delta(\lambda)/\mu}$ is the extinction term, ω_0 is the single scatter albedo, $p(\psi_s)$ is the scattering phase function, δ is optical depth, θ_0 is the sun zenith angle, Φ_0 is the sun azimuth angle and μ is cosine of the satellite zenith angle (θ). Solving for the radiance due to aerosol scattering becomes:

$$L_a = \frac{\omega_0}{L(\theta_0,\phi_0,\lambda)}\,p(\psi_s)\delta_a \,, \qquad (2.3)$$

where δ_a is aerosol optical depth. This reduced transfer equation is based on the following assumptions: the region is sun glint free, the aerosols are spherical and non-absorbing and single scattering dominates (Durkee et al, 1991). This model was applied to the QuickBird imagery to determine aerosol optical depth (AOD).

B. OPTICAL PROPERTIES OF THE OCEAN

Knowledge of the radiance within and leaving the water column is a prerequisite to deriving a depth value from L_t corrected for atmospheric attenuation and scattering. If the optical properties of water are known and bottom reflectance is uniform, a good correlation between water depth and a waveband can be assumed (Lyzenga, 1985).

Several constituents of water significantly alter the scattering and attenuation of radiation in the visible and near-infrared spectrum. Salts increase scattering by 30% in comparison to fresh water but have little effect on absorption. Raman scattering generates many different wavelengths of light from a nominally single-wavelength source through interaction with molecules within the water column. Organic compounds (or yellow matter) and Coloured Dissolved Organic Matter (CDOM) are created by decaying plant matter. CDOM is a significant absorber of the blue waveband. Inorganic particulate matter such as fine minerals from estuarine outlets can scatter visible light. Organic particulate matter, including chlorophyll, viruses, bacteria, phytoplankton and organic detritus can, depending on their concentration and size, scatter visible light appreciably (Fisher, 1999).

The surface morphology of the sea surface also affects the radiance of light from the water column. Ripples and waves alter the reflective properties of the sea surface and introduce variability, or noise, in the received radiance values at the sensor (Clark, 2005).

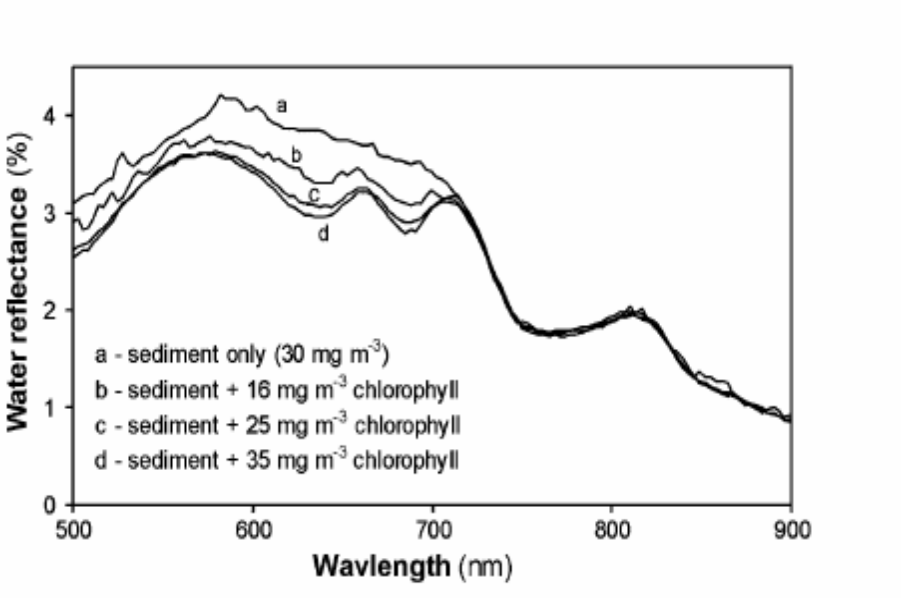

Figure 2. Water reflectance spectra measured by spectro-radiometer with varying chlorophyll amounts. (From: Lavender et al, 2004).

The sum of spectral absorption and scattering coefficients are termed the Inherent Optical Properties (IOPs) of water and are related to the constituents of the water column. The spectral absorption coefficient is the fraction of incident power at a given wavelength that is absorbed per unit distance in a medium. The spectral scattering coefficient is the amount of incident power per unit distance that is scattered out of the beam (Mobley, 1995). Whereas IOPs are dependent on the medium alone, Apparent Optical Properties (AOPs) are dependant on the directionality of radiance. The spectral radiance reflectance (R_s) is the ratio of spectral upwelling irradiance to spectral downwelling irradiance at a given depth:

$$R_s(z,\lambda) = \frac{E_u(z,\lambda)}{E_u(z,\lambda)}, \qquad (2.4)$$

where z is depth, λ is wavelength, E_u is upwelling irradiance and E_d is downwelling irradiance. Spectral remote sensing reflectance (R) is the ratio of water leaving radiance (L_w) to downwelling irradiance (E_d) and is calculated just below the surface:

$$R(0-) = \frac{E_u(0-,\lambda)}{E_d(0-,\lambda)}, \qquad (2.5)$$

where (0-) denotes some small depth just below the water's surface. This value is the amount of downwelling light that leaves the surface after interacting with the water column and the seabed and is recorded by the remote sensor (Fisher, 1999).

C. THE RADIATIVE TRANSFER EQUATION

To determine water depth from satellite-recorded radiances, atmospheric and water column radiative transfer properties are summed and the result is solved for water depth. There are three main methods:

1. Linear Method

Linear methods use the assumption that light attenuates as a power law in water to determine depth (Lyzenga, 1978; Jupp, 1988; Philpot, 1989) and that this attenuation is spatially homogeneous. Philpot (1989) states:

$$L_d = L_b^{-gz} + L_w, \qquad (2.6)$$

where L_d is the radiance observed at the remote sensor, L_b is the bottom reflected radiance, g is the water attenuation coefficient, z is depth and L_w is the radiance over optical deep water. The assumption is that atmospheric transmittance, path radiance, sea state, water reflectance, bottom reflectance, and water attenuation are constant. In order to incorporate atmospheric and water column optical properties, this formula is rearranged to give:

$$L_d(z) = CE_d(0-)(Ab - \rho_\infty)^{-gz} + CE_d(0-)\rho_\infty + L_{sg} + L_{path}, \qquad (2.7)$$

where C is the atmospheric transmission factor, $E_d(0-)$ is downwelling irradiance just below the water surface, A_b is bottom reflectance (albedo), ρ_∞ is the irradiance reflectance of optically deep water, L_{sg} is the sun glint and L_{path} is the path radiance. The atmospheric and sun glint terms are removed and the radiance values are converted to top-of-the-atmosphere values. Melsheimer and Liew (2001) state:

$$R(z) = \frac{1}{g}\left[R(0) - R(\infty)\right]^{-gz} + R(\infty), \qquad (2.8)$$

where R is top-of-the atmosphere reflectance. Equation 2.8 is then solved for depth:

$$z = \frac{1}{g}\left(\log\left[R(z) - R(\infty)\right] - \log\left[R(0) - R(\infty)\right]\right), \qquad (2.9)$$

2. Ratio Method

Ratio methods build on the assumption that light attenuates exponentially with water depth by comparing the ratio of different attenuation rates between wavebands to determine depth. As depth increases, the water leaving radiance of a band with higher absorption (green) will decrease proportionately faster than that of a band with lower absorption (blue) and the ratio of blue to green values will therefore increase (Stumpf and Holderied, 2003). The basis of the ratio transfer equation is the linear relationship presented by Lyzenga (1985) that states:

$$Z = a_i X_i + a_j X_j + Z_0, \qquad (2.10)$$

with:

$$X_i = \ln\left[R(\lambda_i) - R_\infty(\lambda_i)\right], \qquad (2.11)$$

where R is the reflectance at wavelength (λ_i), R_∞ is the reflectance of optically deep water at wavelength (λ_i), and a_i, a_j and Z_0 are coefficients that account for the optical properties of the water. This is combined as a ratio of two wavelengths by Stumpf and Holderied (2003) to give:

$$Z = m_1 \frac{\ln(nR_w(\lambda_i))}{\ln(nR_w(\lambda_j))} - m_0, \qquad (2.12)$$

where m_1 is a tunable constant to scale the ratio to depth, n is a fixed constant for all areas to ensure the terms remain positive and m_0 is an offset for a reference depth of 0m (the Z_0 term in equation 2.10). The theoretical benefit of a ratio transform is a compensation for variable bottom reflectance. It is claimed a change in bottom albedo affects both bands similarly, but a change in depth affects the higher waveband more, so variable bottom types can be analysed more accurately.

3. Stratified Genetic Algorithm

The Stratified Genetic Algorithm (SGA) is a development of the Depth of Precision (DOP) model proposed by Jupp (1988) that states:

$$Z = \sum_{i=1}^{N} \frac{\ln(L_e)_i}{-2k_i N} - \sum_{i=1}^{N} \frac{\ln(L_b)_i}{-2k_i N}, \qquad (2.13)$$

L_e is measured radiance at the sensor, L_b is radiance from the seabed, k is the absorption coefficient of the water and N is the number of spectral bands. The second term is removed and replaced with a regression coefficient (Y_j) by Gianinetto and Lechi (2003) to give:

$$z = \sum_{j=1}^{m} \frac{\ln(L_e)_j - Y_j}{-2k_j}, \qquad (2.14)$$

where m is the number of layers. The SGA method divides the water column into levels of increasing depth and computes k_j and Y_j for each in order to calculate water depth. This algorithm is repeated for all spectral wavebands and those with a high correlation coefficient are used to determine depth.

THIS PAGE INTENTIONALLY LEFT BLANK

III. DATA

A. DATA DESCRIPTION

The data used includes Digital Globe's QuickBird (QB) polar orbiting satellite image retrieval system, LIDAR bathymetry soundings, United Kingdom Hydrographic Office (UKHO) and National Geophysical Data Centre (NGDC) hydrographic chart data, and the HYDROLIGHT water coefficient model.

B. INSTRUMENTS

1. QuickBird Data

The QB 2 satellite is a polar-orbiting, sun-synchronous satellite operating at an altitude of 450 kilometers with a 98-degree inclination on a 93.4 minute orbit cycle with a 10:30 a.m. local equator crossing time for the ascending node (Digital Globe, 2004). The satellite captures solar reflected energy in four spectral bands in a swath 16.5km wide.

CHANNEL	BANDWIDTH (nm)	SPATIAL RESOLUTION(m)
1	450-520	2.44-2.8
2	520-600	2.44-2.8
3	630-690	2.44-2.8
4	760-900	2.44-2.8

Table 1. QB bandwidth and maximum spatial resolutions (DigitalGlobe 2004).

The multispectral bands shown in Table 1 have a nominal spatial resolution of 2.44-2.8m at nadir and in addition a panchromatic band (not shown) that has a nominal resolution of 0.6m meters. The QB data was acquired by the National Geospatial Agency (NGA) after being processed and geo-referenced by DigitalGlobe ground stations.

Figure 3. Digital Globe's QB imagery of Plymouth Sound. (After: DigitalGlobe, 2005).

2. LIDAR Data

Light Detection and Ranging (LIDAR) determines range records using the time taken for an emitted pulse of energy to hit a target and return to the sensor to determine range. The Scanning Hydrographic Operational Airborne LIDAR Survey (SHOALS) system uses this technology to determining water depth. SHOALS is managed by the Joint Airborne LIDAR Bathymetry Technical Center of Expertise (JALBTCX). The airborne component of the system is installed aboard a DHC/300 Twin Otter airframe and uses a 1064nm primary pulse for an infrared spectra and a 532nm pulse for a blue-green spectra to collect bathymetry data on a 4m grid.

MAXIMUM DEPTH	60 m or 2-3 times Secchi depth
VERTICAL ACCURACY	+/- 15 cm
HORIZONTAL ACCURACY DGPS	+/- 2 m
HORIZONTAL ACCURACY OTF GPS	+/- 0.5 m

Table 2. SHAOLS performance specification (After: http://shoals.sam.usace.army.mil, used 15 Mar 2005).

LIDAR soundings were acquired for Looe Key on 10 December 2004 by JALBTCX and projected to the North American 1988 Datum. The depth of the seabed was calculated below the water surface at the time of data capture. A height of tide correction and datum conversion to WGS 84 is made before comparison with satellite derived depths.

3. UKHO and NGDC Hydrographic Data

Satellite depth analysis is also compared to navigation chart data supplied by the UKHO for the Plymouth and the NGDC for the Looe Key area. These products comply with the International Hydrographic Organisation (IHO) standards for hydrographic surveys of Order 1. This order is required for harbours, harbour approach channels, recommended tracks, inland navigation channels, and coastal areas of high commercial traffic density (less than 100m) with depths up to 100 m (S44 IHO 1998). The basic assumption is that errors are classified by: a, the sum of all dept-independent errors and b, the sum of all depth-dependent errors, expressed as a percentage of water depth. The degrees of accuracy required are divided into four categories depending on the product to be manufactured. The inshore navigation charts used in this study comply with the Category 1 specification outlined in Table 3.

ORDER	SPECIAL	1	2	3
Depth of uncertainty for reduced depths (95% confidence level)	a = 0.25m b = 0.75%	a = 0.5m b = 1.3%	a = 1.0m b = 2.3%	a = 1.0m b = 2.3%
Bathymetric model uncertainty (95% confidence level)	a = 0.25m b = 0.75%	a = 1m b = 2.6%	a = 2m b = 5%	a = 5m b = 5%

Table 3. Summary of Minimum Standards for Depth Uncertainties. (After: S44 IHO 1998).

The UKHO charts are projected to the WGS 84 datum, whereas the NGDC chart is projected onto the North America Datum of 1983. NGDC depths were corrected to WGS 84 before depth comparisons with QB derived depths were made. Because QB imagery is processed to WGS 84, the NGDC depths were corrected to WGS 84 before depth comparisons with satellite derived depths were made.

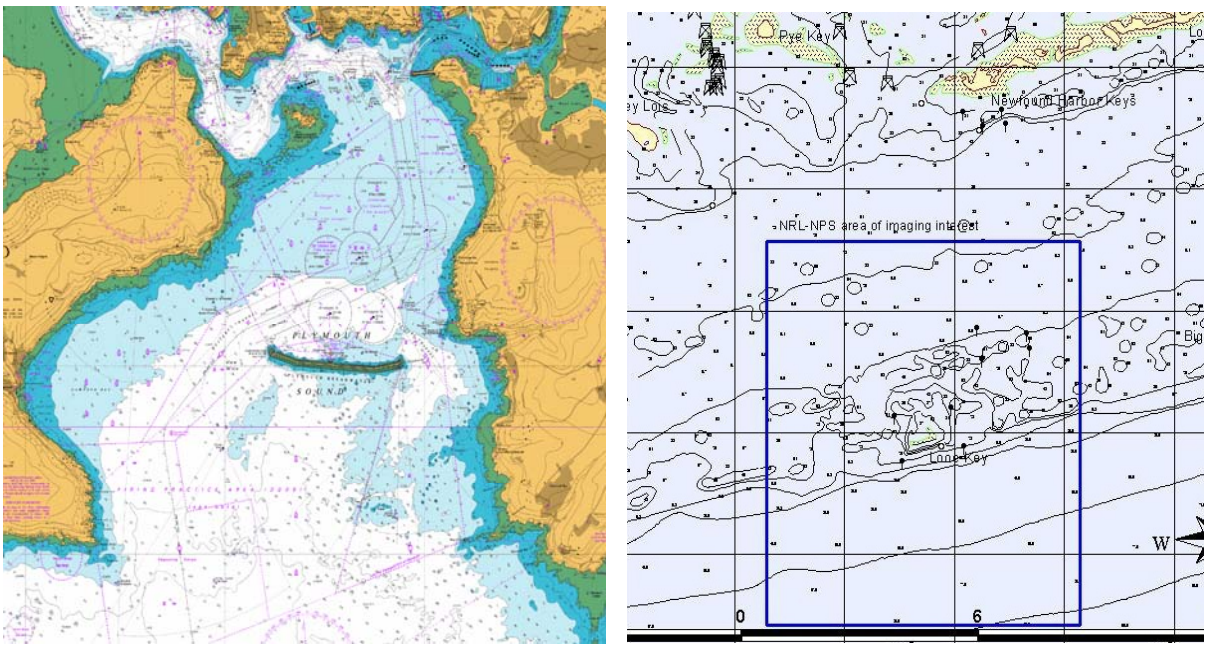

Figure 4. Nautical charts for Plymouth Sound and Looe Key (After: UKHO, NGDC).

4. HYDROLIGHT

The HYDROLIGHT radiative transfer numerical model computes radiance distributions and related quantities including irradiances, reflectances and diffuse attenuation functions of the water column. Inputs from the user include the water absorption and scattering properties, the sun and sky radiances, and the bottom characteristics. The output includes the water-leaving radiance and remote-sensing reflectance of the water column, known as *K*-functions. To solve for water depth, the downwelling attenuation coefficient output (K_d), is determined for the QB wavebands channels used and incorporated into the various depth algorithms.

A classification scheme has been developed for oceanic waters based on the value of K_d (Jerlov, 1976). The three different optical types, Case I, Case II, and Case III classify the increase in attenuation, scattering and absorption of photons with differing levels of turbidity. Case I (divided into IA and IB) are the clearest and Case III being the most turbid. The HYDROLIGHT 3.0 version is used to determine K_d for Case I and Case II waters. The Case II waters are used for Plymouth Sound with an observed value for chlorophyll concentration, via a separate FORTRAN sub-routine, and supplied values for CDOM and Raman scattering. Case I water is used for Looe Key where CDOM and particulate matter within the water column is greatly reduced. An averaged value for chlorophyll is used for each area of interest as the lengthy run times for evaluating K_d prohibits evaluating the whole image for a unique value for each pixel.

THIS PAGE INTENTIONALLY LEFT BLANK

IV. METHODOLOGY

A. ATMOSPHERIC CORRECTION

The amount of energy received by a remote sensor from atmospheric aerosol effects and surface reflectance adds to the amount of energy radiated from the water column and seabed and must therefore be calculated and corrected for. Aerosol characterisation information is acquired from in situ or remote methods. In situ measurements are made using ground or air based radiometers, sun-photometers and spectrometers, and provide high resolution data for highly defined areas. Remotely sensed methods, such as those used with the Sea-viewing Wide Field-of-view Sensor (SeaWIFs) remote sensing system, use satellite mounted radiometers that provide an analysis over a large spatial area at lower resolution. Without access to in situ measurements, aerosol optical depth (AOD) of the atmosphere is calculated from the QB imagery using the over-water dark object approach and the NPS Aerosol Model. Sun glint and other reflectance effects are corrected for using a near infrared (NIR) scaling algorithm applied to the QB imagery.

1. NPS Aerosol Model

The NPS Aerosol Model applies linearised single scatter theory to an estimate of bidirectional surface reflectance using scattering phase functions that are parameterized into seven aerosol model size distributions (Durkee et al, 1991). The aerosol model sizes are based on those typically found in a marine environment and a particle size parameter, called S12, is calculated using the ratio of the red and NIR wavelength radiances. The S12 value and scattering angle are used to determine aerosol model index (AMI), and Mie theory is used to calculate scattering phase function curves for each aerosol model size distribution. The AMI and scattering angle determine the scattering phase function that is needed to calculate AOD.

The NPS Aerosol Model was designed for use with NOAA-14 AVHRR radiance values. In order to apply the model to the different wavebands of the QB data, the radiance values are adjusted. The NOAA-14 AVHRR radiances were linearly

extrapolated to match the effective center red and NIR wavelengths of the QB wavebands. The linear extrapolation method is considered parsimonious due to the linear nature of in-band solar irradiance and nearly linear nature of the scattering mechanisms at the two wavelengths. The extrapolated model radiances were used in the NPS Aerosol Model as the input for top of the atmosphere radiance. The output values for QB red and NIR central wavelengths for the respective wavebands were then extrapolated linearly to the blue, green and red waveband central wavelengths. The retrieved aerosol optical depths for each area are presented in Table 4.

LOCATION	**BLUE AOD**	**GREEN AOD**	**RED AOD**	**NIR AOD**
Plymouth Sound	0.3778	0.2311	0.1468	0.0090
Looe Key	0.3019	0.2617	0.231	0.1028

Table 4. NPS Aerosol Model values of AOD for QB imagery.

2. Sea Surface Correction

The high resolution of QB imagery increases the incidence of quasi-stochastic sea surface effects, caused by ripples and waves, which creates specular reflectance. This acts as a significant source of additional energy received at the remote sensor. An increased surface wind results in greater scattering and creates glint that partially obscures the water leaving radiance that is fundamental in determining water depth. The Sea Surface Correction algorithm (Hochberg et al., 2003) is used to eliminate the majority of the wave and glint effects. This model utilises the NIR waveband, which exhibits the maximum absorption and minimal water leaving radiance over clear waters, to characterise the spatial distribution of relative glint intensities. It is assumed that although absolute glint intensity varies with wavelength, relative glint intensity is constant across NIR and visible wavelengths. The NIR corrected glint distribution is scaled in the blue, green and red QB wavebands, and the respective results are subtracted from the measured radiances to remove glint effects. Uncorrected and corrected images for Looe Key can be seen in Figs. 5 and 6.

Figure 5. Image of Looe Key before sea surface correction was applied showing ripples on the sea surface.

Figure 6. Image of Looe Key after sea surface correction applied with rippling removed.

3. Conversion to Reflectance Values

After removing the aerosol and glint effects, the resultant QB imagery is converted from radiance values to reflectance values using Eq. 4.1 for use in the various depth retrieval algorithms:

$$R = \frac{\pi R_s}{E_0} \tag{4.1}$$

where R is reflectance, R_s is surface radiance value and E_0 is the incoming solar irradiance.

B. WATER COLUMN CORRECTION

The effective attenuation coefficient of the water mass must be determined in order to relate the water depth to the reflectance values received at the sensor. The HYDROLIGHT model is used to determine a value for the attenuation coefficient based on a value of chlorophyll determined using the QB imagery.

1. Chlorophyll Analysis

The amount of chlorophyll in each image is calculated by determining the relative chlorophyll levels and converting this to a concentration figure. Radiance at all wavelengths decreases with an increase in chlorophyll concentration and this rate of decrease differs between wavebands. The rate of decrease is more rapid for blue than green wavelengths. A relative value for chlorophyll concentration can be derived from a ratio of the reflectance at the blue and green wavelengths. The spatial distribution of the chlorophyll concentration can be seen for each area in Figs. 7 and 8.

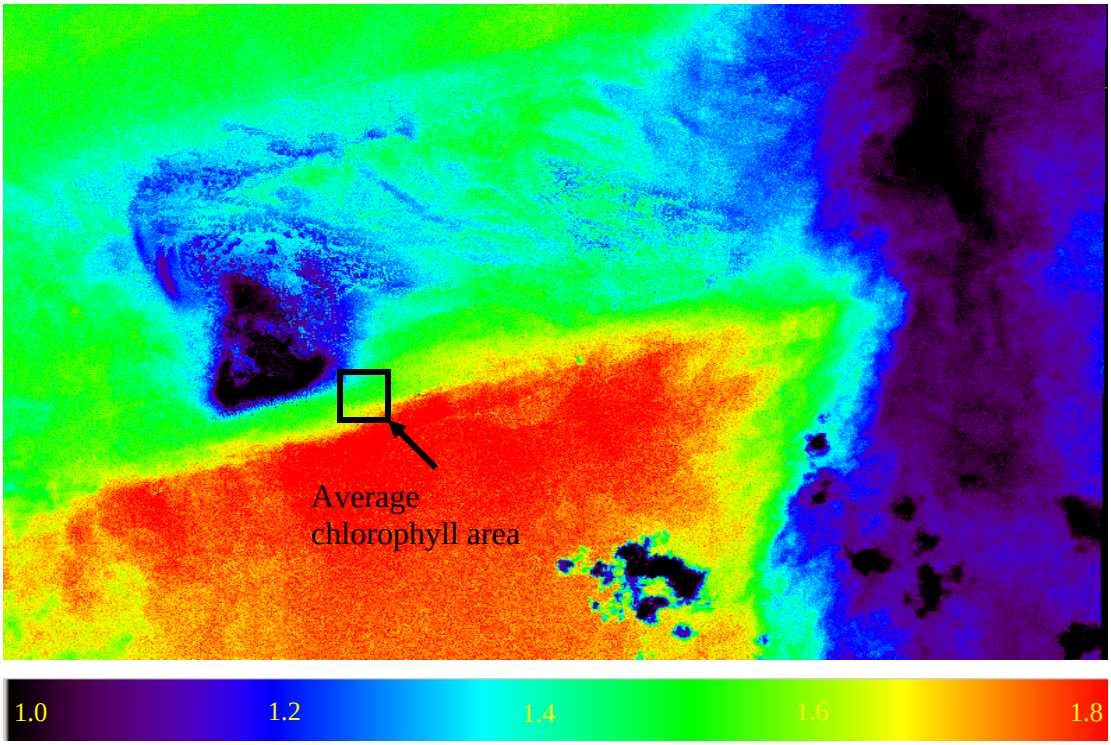

Figure 7. Looe Key ratio of blue/green wavebands (relative chlorophyll content) derived from QB imagery.

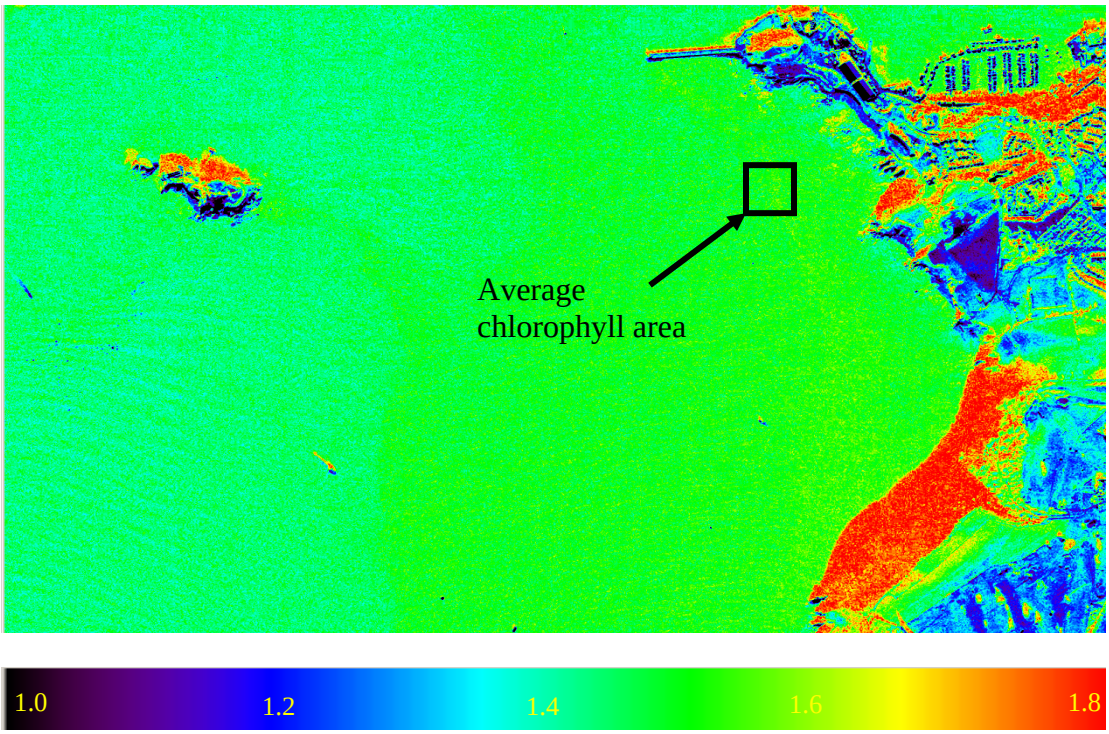

Figure 8. Plymouth Sound ratio of blue/green wavebands (relative chlorophyll content) derived from QB imagery.

The ratio values are then be converted to a concentration amount using a pigment algorithm for Case 1 and 2 waters (Gordon and Clark, 1981):

$$Chl = A\frac{\lambda_i}{\lambda_j}^{B} \qquad (4.2)$$

where Chl is the chlorophyll concentration (mg/m^3), A and B are constants, λ_i and λ_j are the blue waveband radiance and green waveband radiances respectively. The variability in concentration values across each study area is resolved by selecting one area in each image where depth calculations are to be carried out and an average value determined for input into the HYDROLIGHT model. The retrieved chlorophyll concentrations are shown in Table 5 for the areas shown in Figs 7 and 8.

AREA	**CHL (mg/m^3)**
Plymouth Sound	0.303
Looe Key	0.266

Table 5. Calculated chlorophyll concentrations for study areas.

2. HYDROLIGHT

The wavelength dependent attenuation coefficient, $K_{d,}$ is required to derive depth using the linear and the stratified genetic algorithms. These were modeled using HYDROLIGHT 3.0 and incorporating pre-defined settings for Case 1 water for Looe Key and Case II water for Plymouth Sound. A separate FORTRAN subroutine was used to fix the value of chlorophyll at the given concentrations for each area, as HYDROLIGHT would allow the chlorophyll content to vary with depth otherwise.

The HYDROLIGHT input parameters were average chlorophyll concentration, pressure, temperature, humidity, visibility, precipitation, longitude, latitude, wavelength, solar zenith angle and satellite zenith angle. The output presented in Table 3 shows that as wavelength increases so does $K_{d,}$ as would be expected due to higher absorption of visible light by water at longer wavelengths. The chlorophyll and CDOM amounts at

Plymouth Sound were significantly higher than Looe Key, and this is reflected in the higher attenuation values at these locations.

The HYDROLIGHT results were compared with empirically observed K_d values. These were derived from re-arranging the linear depth algorithm at known depths to solve for K_d. The HYDROLIGHT results are shown in Fig 9.

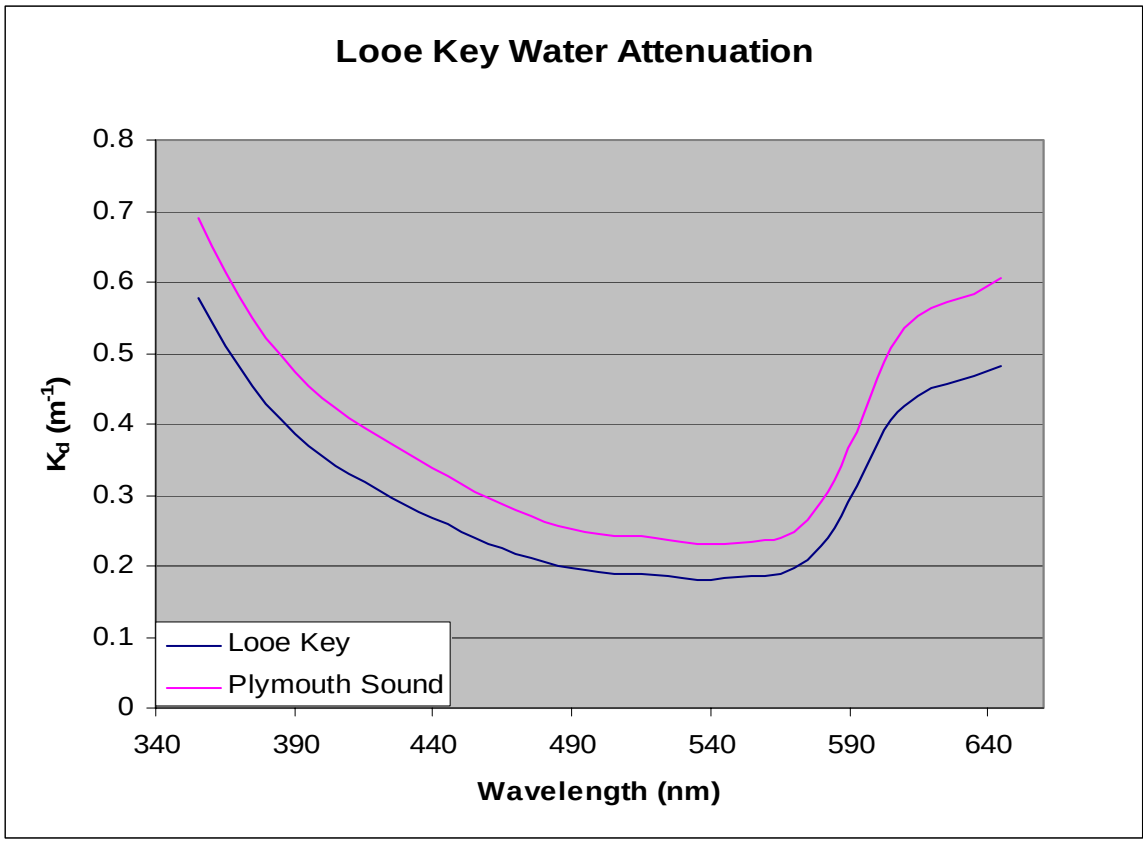

Figure 9. HYDROLIGHT derived water attenuation coefficient (K_d) for each area.

C. DEPTH RETRIEVAL

An analysis of the stratified genetic and linear algorithm revealed that both models were based on the same derived form of the radiative transfer equation. The stratified genetic algorithm differs from the linear algorithm by incorporating a regression analysis-derived coefficient for the second term of the linear algorithm:

$$z = \frac{1}{g}\left(\log\left[R(z) - R(\infty)\right] - \log\left[R(0) - R(\infty)\right]\right) \qquad (2.9)$$

$$z = \sum_{j=1}^{m} \frac{\ln(L_e)_j - Y_j}{-2k_j} \qquad (2.14)$$

where k_j the water attenuation coefficient and g is $2k_j$, L_e and R(z) are the measured reflectance values and Y_j, and R(∞) are the measured reflectance values over optically deep water. The coefficient Y_j was determined by empirical analysis using known depths along each transect. The stratified genetic algorithm was used in comparison with the ratio algorithm to retrieve depths for each area.

1. Ratio Transfer Algorithm

The ratio algorithm requires empirically derived coefficients to normalise the natural log of the ratio of green to blue reflectance values to retrieve a depth term and then reference those depths to the sea surface. The first coefficient, m_1, is a tunable constant to scale the ratio to a relative depth in meters. The second coefficient, m_2, is an offset value to reference the first term to 0m depth. The ratio algorithm assumes that "a change in bottom albedo affects both bands similarly, but changes in depth affect the high absorption band more".[1] A regression algorithm was used with two known depths from each area to determine respective values of m_1 and m_2 respectively.

In the turbid Plymouth Sound waters, the blue waveband was scattered to such an extent that valid radiance values were not possible for use in the ratio algorithm. To resolve this problem, the radiance levels for each waveband were analysed along a 440m transect in the estuarine waters of the Sound. The results, detailed in Figs 10-12, show that the blue waveband is scattered significantly and no discernable correlation can be made between an increase in depth and reduction in radiance value. The green waveband shows a degree of decay in value with increased depth along the transect, and the red band shows the greatest amount of response to depth. The effect of scattering by CDOM

1 Determination of water depth with high-resolution satellite imagery over variable bottom types. Stumpf and Holderied. American Society of Limnology and Oceanography, 2003.

and particulate matter in the red and green waveband is less than in the blue, so therefore, it is proposed that an amendment to the ratio technique is employed in turbid waters, namely, the use of the green to red reflectance values. In this analysis the standard ratio method was used for Looe Key and the amended version for Plymouth Sound.

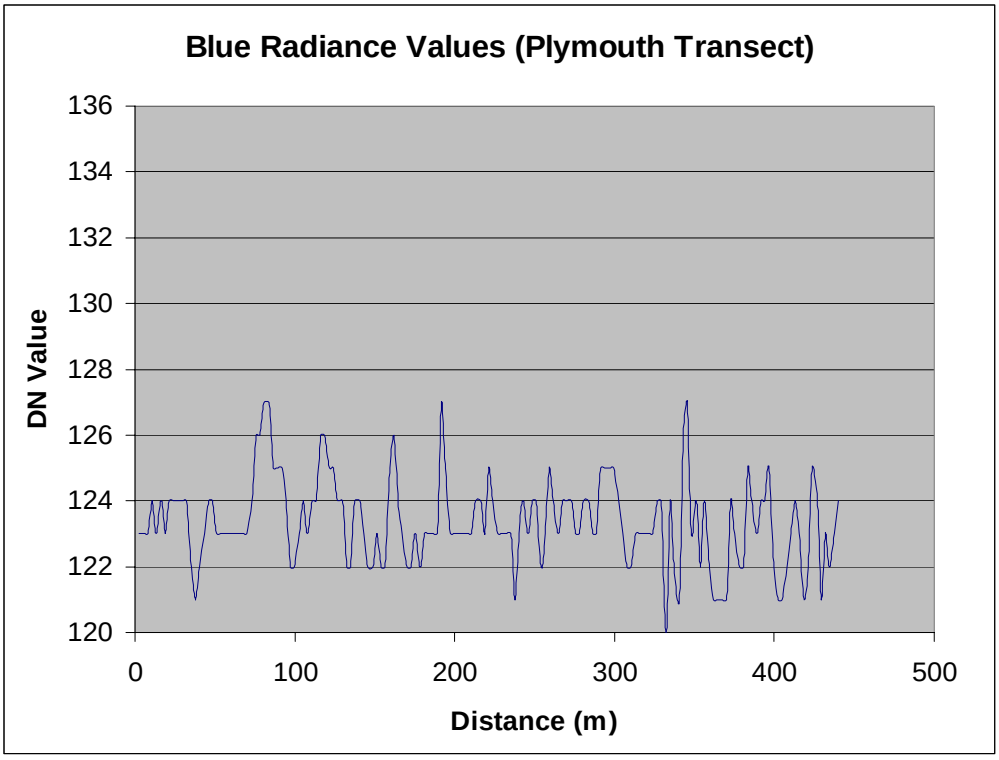

Figure 10. Digital Number (DN) radiance values for QB blue waveband.

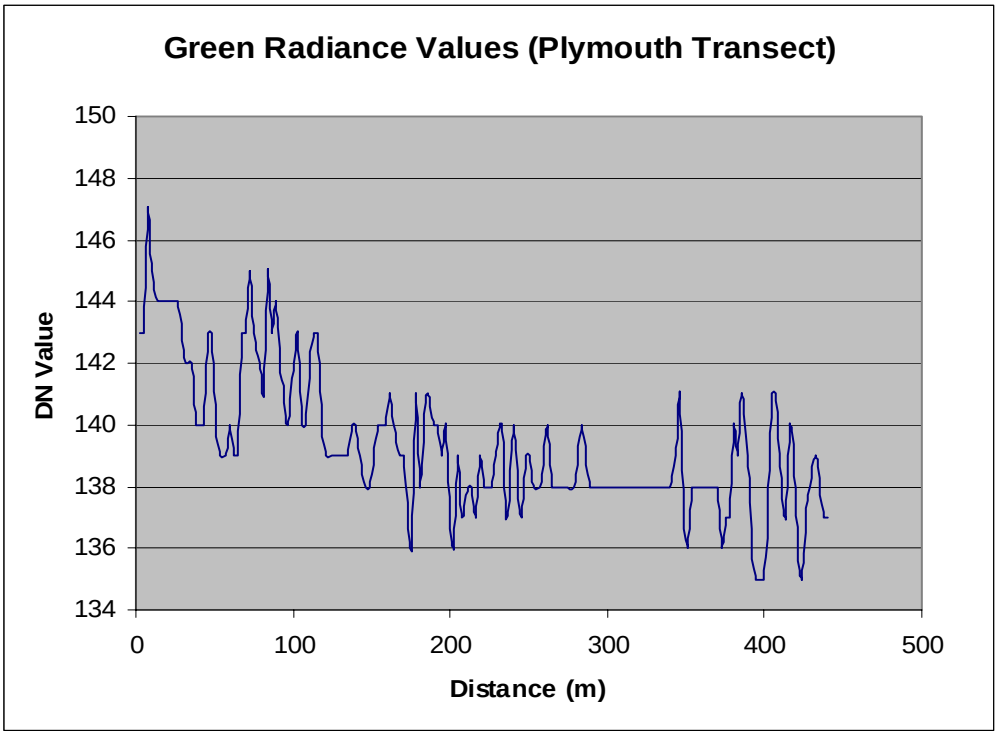

Figure 11. DN radiance values for QB green waveband.

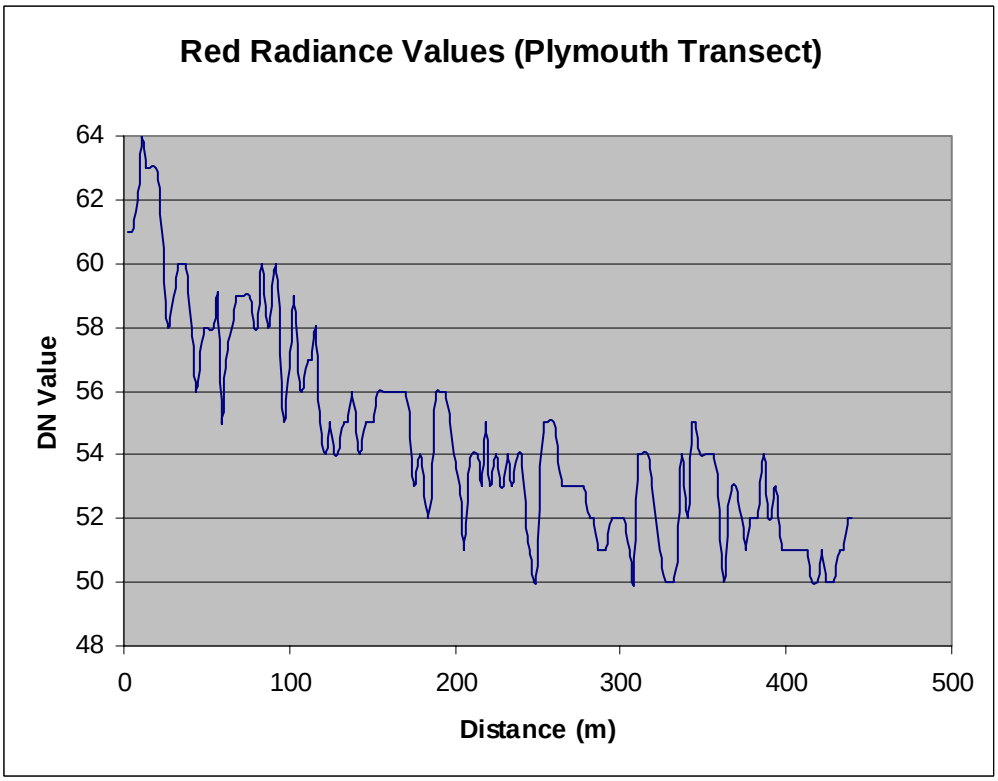

Figure 12. DN radiance values for QB red waveband.

2. Stratified Genetic (Turbidity) Algorithm

The second term of the genetic algorithm, $Y_{j,}$ was derived through a regression analysis in a similar manner to the ratio method. Bottom reflectance values for each wavelength were taken from the QB images where the wet bottom type was exposed, or lay a few centimeters beneath the water's surface. The area for analysis in each image featured a predominantly sand bottom type. This value was incorporated into a term that included bottom albedo and the reflectance value of optically deep water:

$$Y_j = \frac{\ln[\frac{1}{\pi} R_b - R_d]}{K_d} \qquad (4.3)$$

where R_b is bottom reflectance and R_d is reflectance of optically deep water.

3. Environment for Visualising Images (ENVI)

The Research Systems Incorporated (RSI) ENVI software package was used to orthorectify and calibrate the QB imagery for accurate comparison with the LIDAR and chart data. The Band Math tool was used to execute the correction algorithms for aerosol optical depth and sea surface reflection and to convert radiance values to reflectance values for each pixel. The two algorithms were then entered into Band Math and executed for each image to calculate depth values for each pixel. Transects were taken within each area for cross comparison with LIDAR and hydrographic chart data.

THIS PAGE INTENTIONALLY LEFT BLANK

V. RESULTS

A. TEST AREAS

To compare the results over a variety of bottom types and depths, a transect was selected within each area, and both the ratio and turbidity algorithms are used to determine water depth along the transect. Accuracy was calculated as the root mean square (rms) error of the derived depths from LIDAR and chart data.

1. Looe Key

The transect at Looe Key extends for 646m in a south-easterly direction from the shallow waters of the key to the edge of a submarine drop off. The depths range from 3.5m at the shallower northwestern end of the transect, increasing to 14.17m towards the drop-off. The bottom types encompass sea grass at the northern end of the line with dark coral fingers roughly two thirds down. LIDAR data is used to assess accuracy with the remotely sensed derived depths. The test transect extending from 24º 32’ 57.53”N, 81º 24’ 10.55”W to 24 32 41.17N, 81º 23’ 55.99”W is shown in Fig 13:

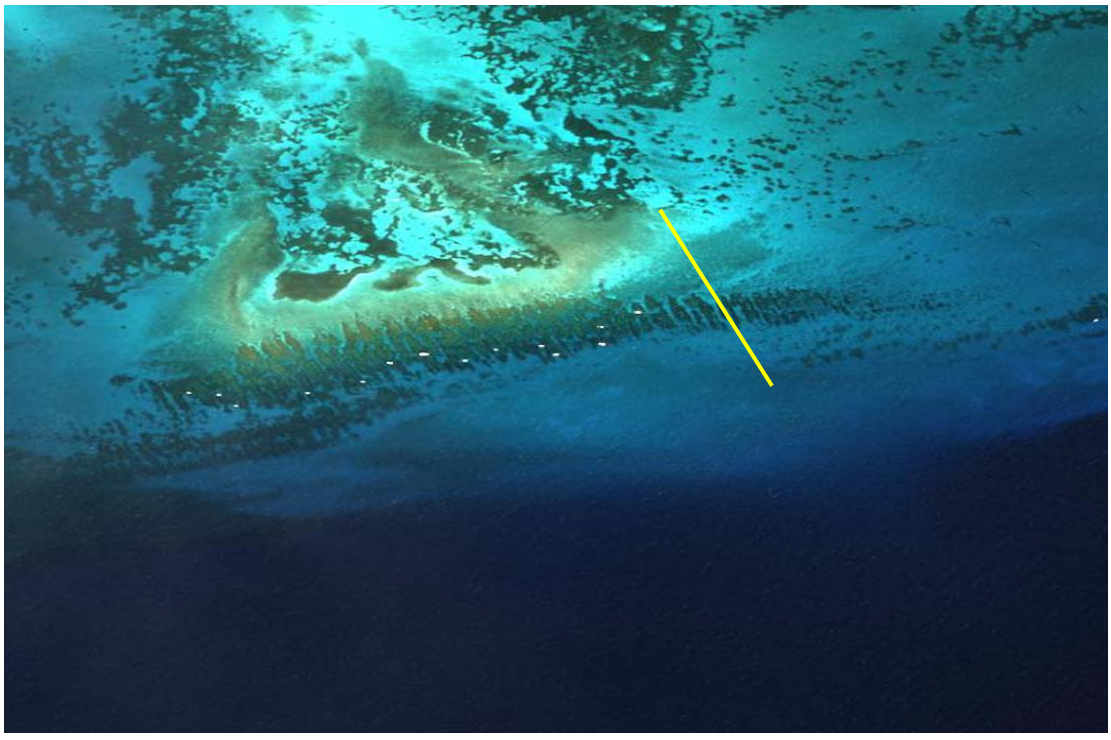

Figure 13. Looe Key test transect.

2. Plymouth Sound

The transect in Plymouth Sound extends 1115.3m in a south-southwesterly direction from the southern shore of Mount Batten Point into the Tamar estuary. The depths range from 0.5m inshore to 10.6m in the estuary. The bottom type was assumed to be sand throughout the area of interest. A third of the way along the transect, a visible band of more sedimentary water was identified. The transect was split into a smaller 368m length that marked the extent of the cleaner inshore water with which accuracy comparisons with chart data were made. The effect of the more sedimentary water was also compared to charted depths. The long test transect extending from 50º 21' 30.12"N, 004º 7' 47.01"W to 50º 20' 54.28", 004º 7' 53.64"W is shown in Fig 14:

Figure 14. Plymouth Sound test transect.

B. DERIVED DEPTHS

1. Looe Key

The QB derived depths using the ratio and turbidity algorithms in comparison with the LIDAR bathymetry are shown in Figs 15 and 16:

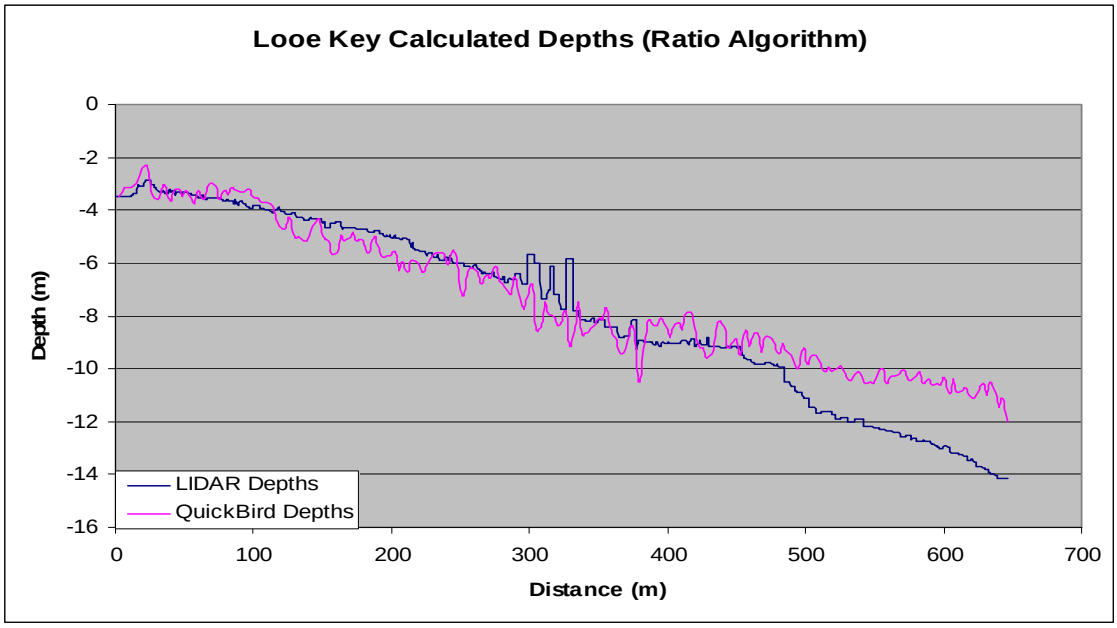

Figure 15. Ratio algorithm and LIDAR bathymetry of Looe Key transect.

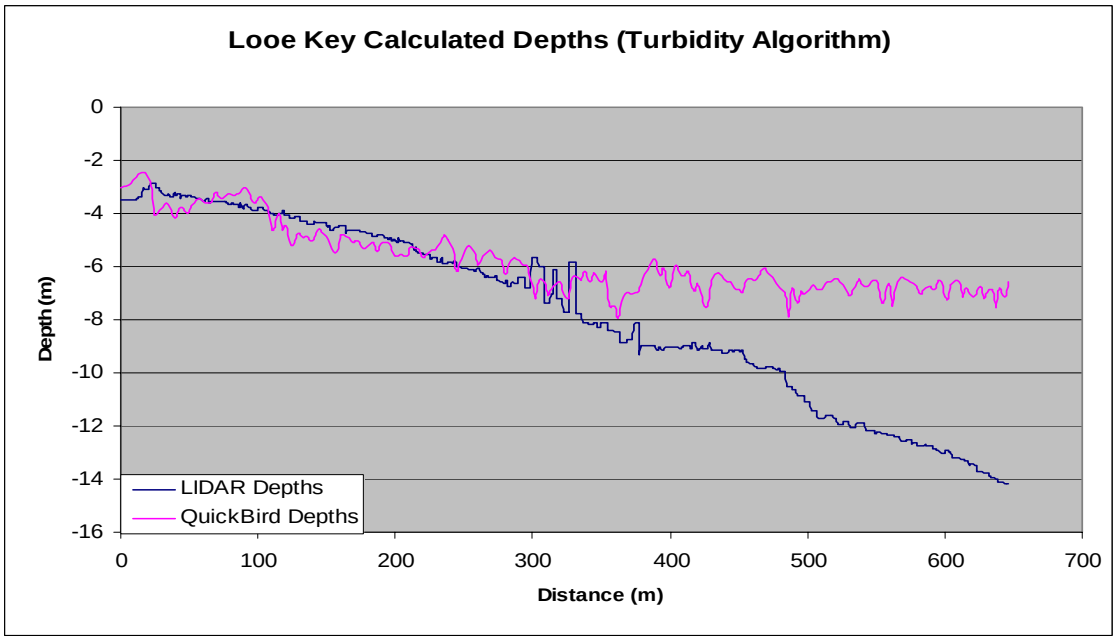

Figure 16. Turbidity algorithm and LIDAR bathymetry of Looe Key transect.

2. Plymouth Sound (Short Transect)

The QB derived depths using the ratio and turbidity algorithms in comparison with chart depths are shown in Figs 17 and 18:

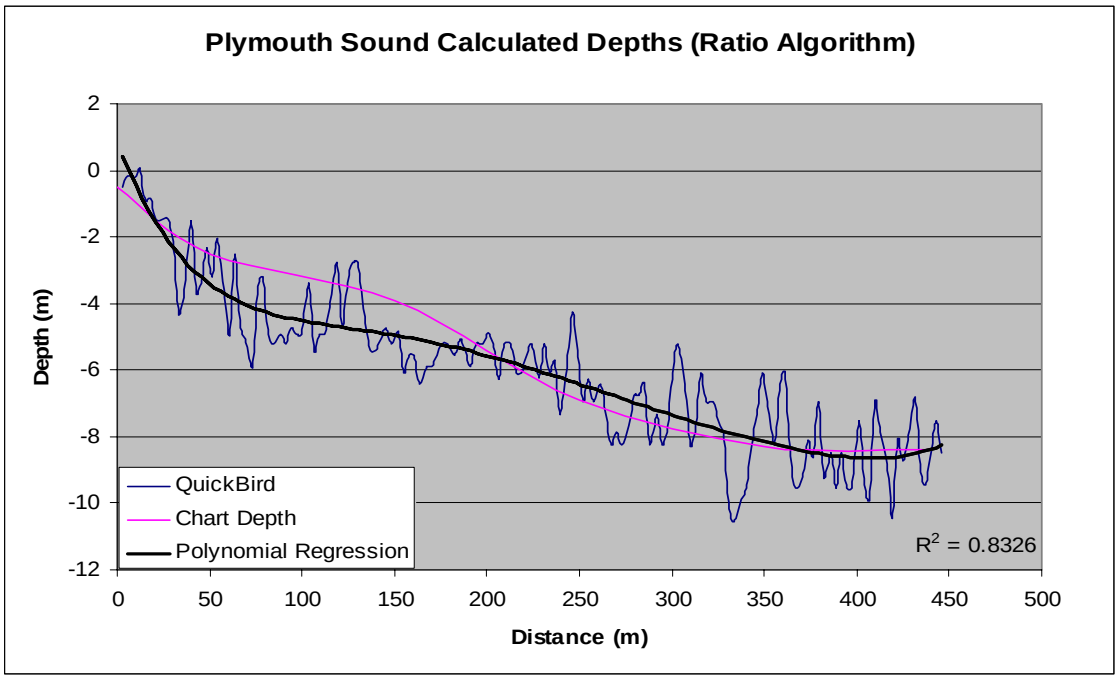

Figure 17. Ratio algorithm and chart depths of short Plymouth Sound transect.

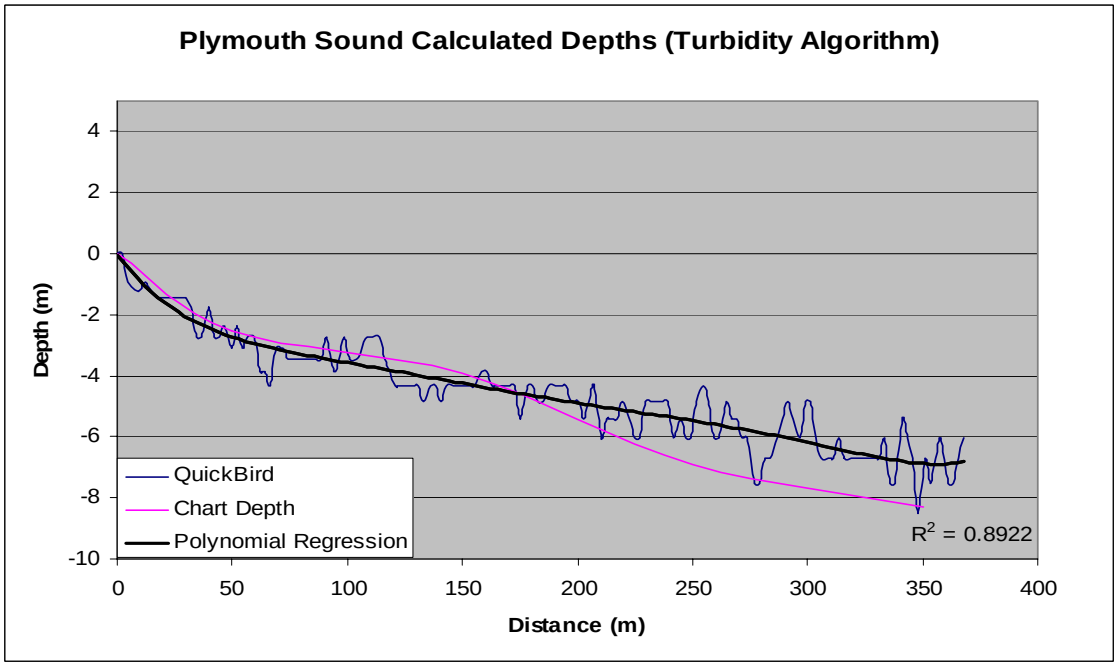

Figure 18. Turbidity algorithm and chart depths of short Plymouth Sound transect.

C. ACCURACY COMPARISONS

1. Looe Key

The results of derived depths at Looe Key from the ratio algorithm produced an average error of 11.7% along the transect, with a maximum error of 38%. Fig 16 highlights the case that as the depth of water increases so to does the inaccuracy of the derived depths. In the case of the turbidity algorithm, the average error is 16.5%, the maximum error is 36.1%. In the case of the ratio algorithm, the greatest discrepancy in depths with the LIDAR data occurs over the darker coral fingers. The turbidity algorithm shows the greatest inaccuracy in water deeper than 7m. The algorithm fails to predict the increasing depth shown on LIDAR. Another source of inaccuracy in both methods is caused by waves and ripples on the sea surface. The higher variability, or noise, in the depth profiles in Figs 16 and 17 is, in part, the result of varying reflection of light caused by these ripples. In general the ratio algorithm (including the discrepancy over the fingers) is more accurate than the turbidity algorithm.

The QB residual accuracies using the ratio and turbidity algorithms in comparison with LIDAR bathymetry are shown in Figs 19 and 20:

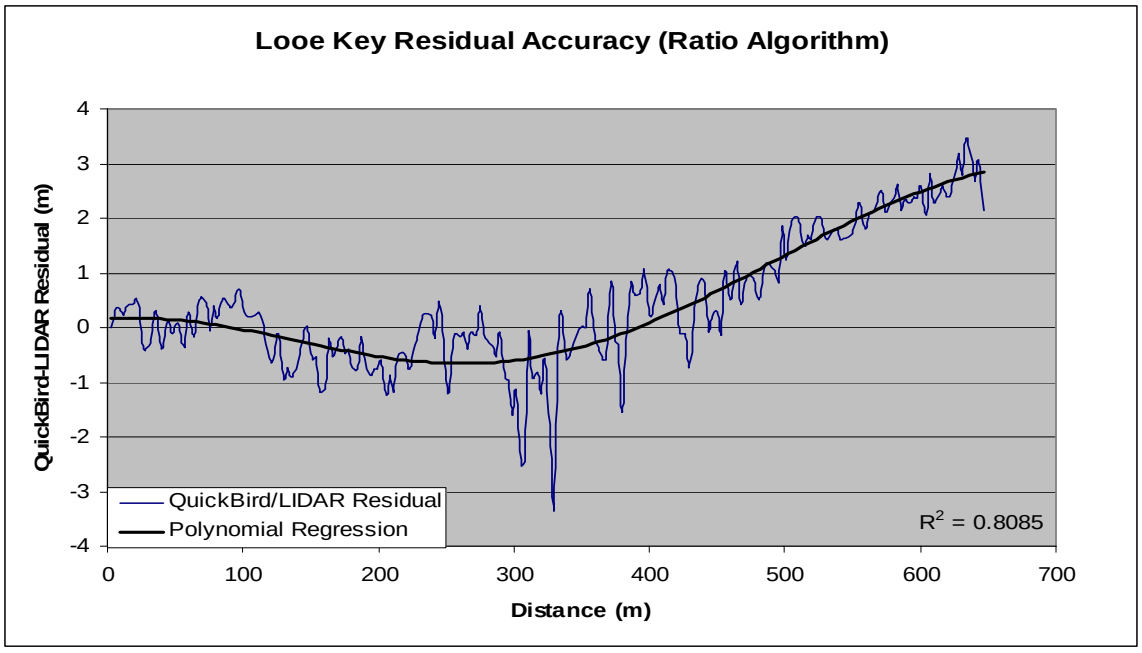

Figure 19. Ratio algorithm/LIDAR residual error of Looe Key transect.

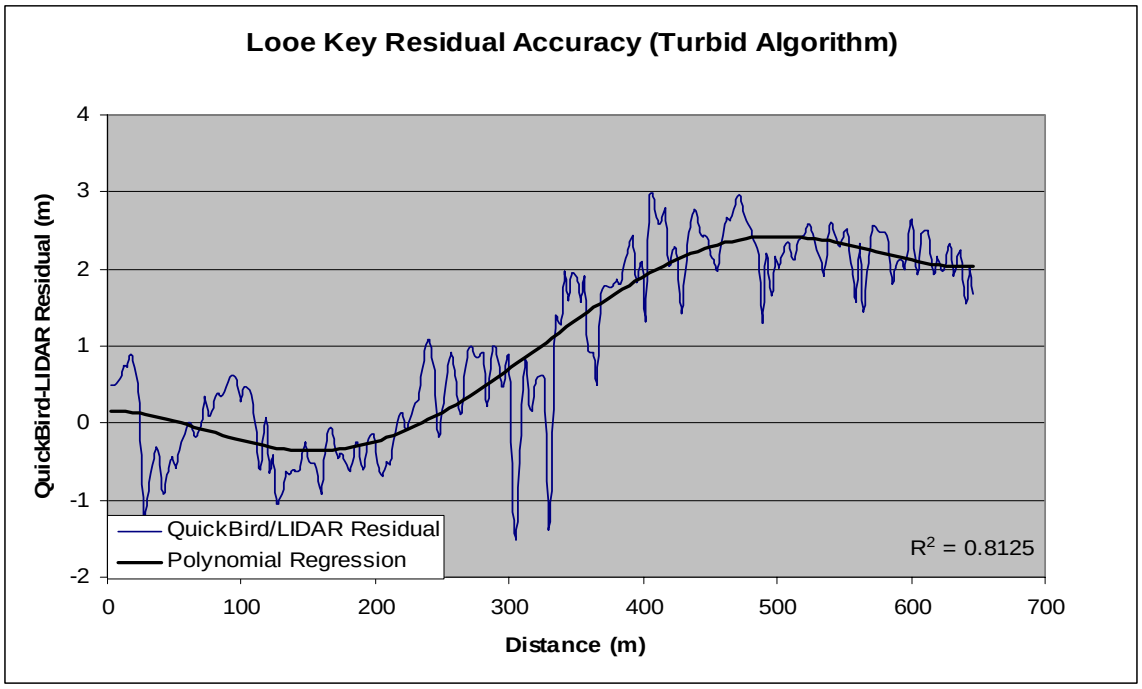

Figure 20. Turbidity algorithm/LIDAR residual error of Looe Key transect.

2. Plymouth Sound (Short Transect)

The results from Plymouth Sound show greater variability and noise for both methods due to the effects of sea surface variability and higher levels of particulate matter in the water column. The amended ratio algorithm average error is 13.1%, with a maximum of 28% and a minimum of 0%. The turbidity algorithm average error is 11.6%, with a maximum of 13% and a minimum of 0.2%. The ratio algorithm does not perform as well as the turbidity algorithm in the shallow water, between 3-5m depth. However, the turbidity algorithm underestimates depths in excess of 5m.

The QB residual errors using the ratio and turbidity algorithms in comparison with chart depths are shown in Figs 21 and 22:

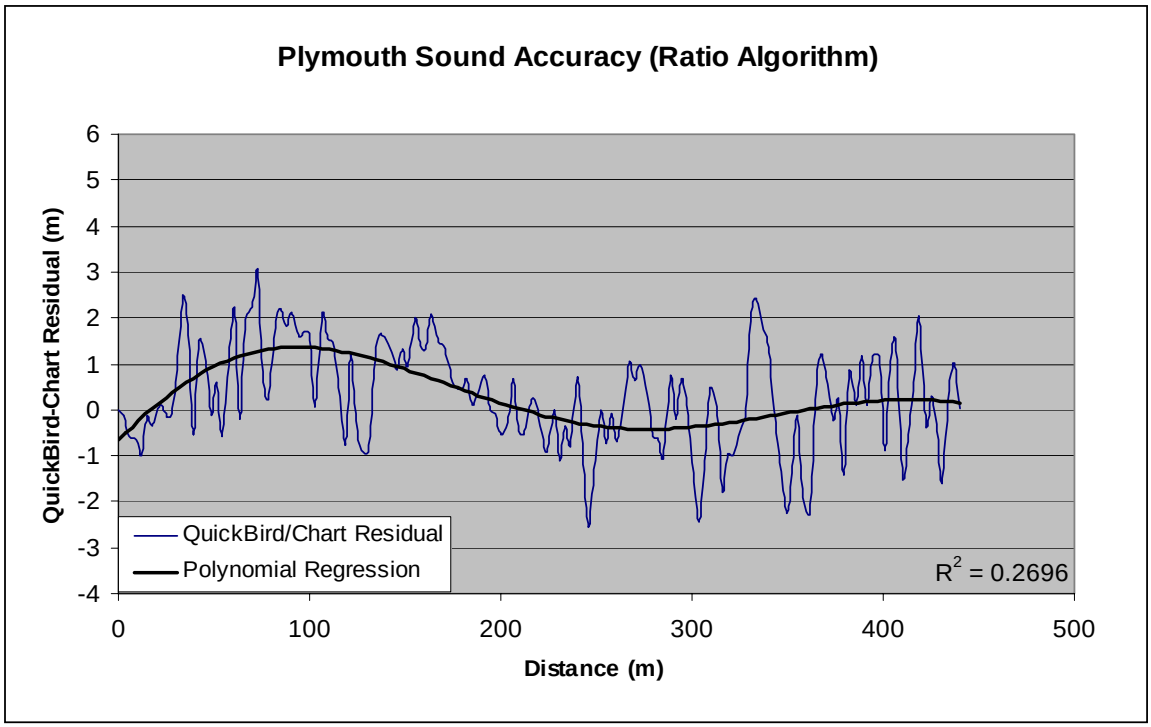

Figure 21. Amended ratio algorithm/chart depth residual error of short Plymouth transect.

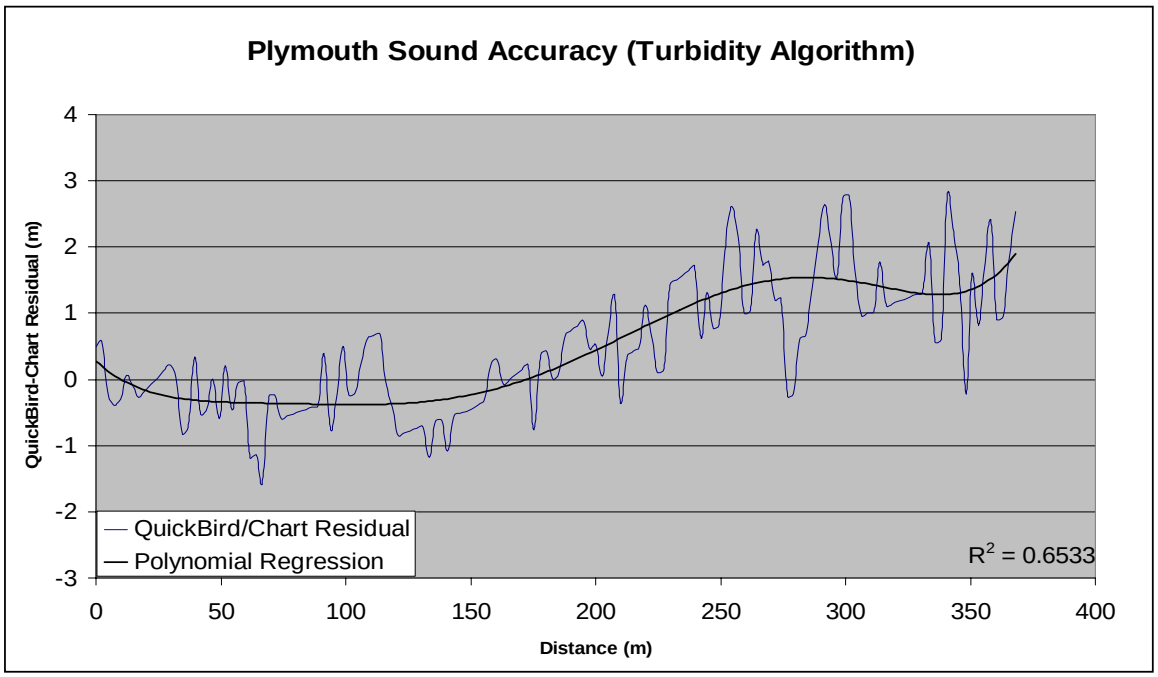

Figure 22. Turbidity algorithm/chart depth residual error of short Plymouth transect.

3. Plymouth Sound (Long Transect)

The effect of increased sedimentary water in Plymouth Sound away from the shore is shown in the longer transect in Fig 23. The chart data show steadily increasing depth as does the turbidity algorithm to a distance of approximately 350m. At this distance a band of more sedimentary water is visible in the QB image (see Fig 14) and the resultant calculated depths plateau to give a set of underestimated values of the charted depth.

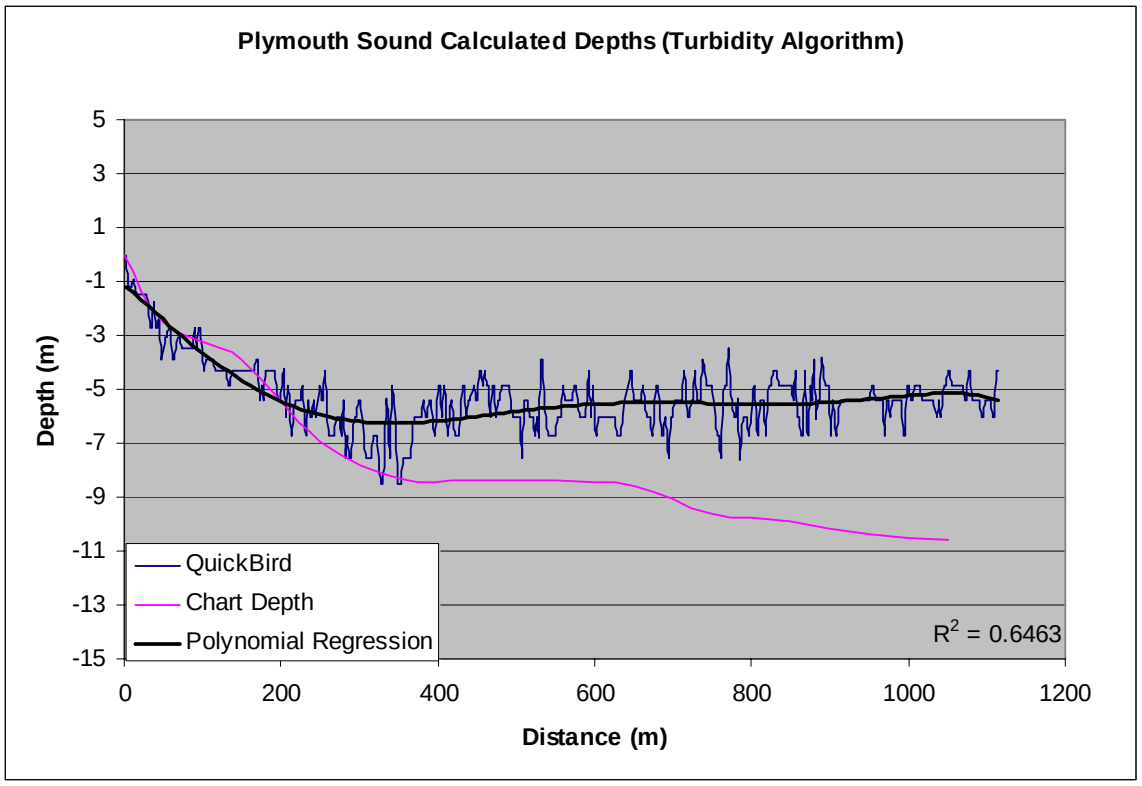

Figure 23. Turbidity algorithm and chart depths of long Plymouth Sound transect.

4. Sources of Error

In summary there are several factors that affect accuracy of the QB remotely sensed bathymetry calculations.

a. Effect of Bottom Type

The coral fingering at Looe Key from approximately 300m to 350m gives a deeper set of values in the ratio algorithm rather than shallower as depicted by LIDAR. The darker colour of the coral fingers is miss-read by the algorithm as deeper water

giving a 38% error in that depth of water. The effects of bottom type and colour do affect the ratio algorithm significantly, and the postulation that the algorithm naturally corrects for bottom type is not supported at Looe Key. The differing bottom reflection propensities of the QB wavebands alter the integrity of the calculated values.

b. Effect of Light Attenuation

The ability of light to penetrate the water column is a limitation for both algorithms. The ratio algorithm returns accurate depths to approximately 10m in the case of Looe Key, whereas the turbidity algorithm is effective to 7m. In Plymouth Sound, the attenuation of light is reduced because the amended ratio algorithm uses the red waveband. The absorption of light by water is greater at the red waveband than at the blue and green (see Fig 10), and therefore, the effective depth penetration is less. The turbidity algorithm bottoms out at approximately 7m as a result. The amended ratio and turbidity algorithms reduce noise in the upper water layers because it is scattered less than the blue or green wavebands. However, it has a reduced operating depth due to the fact that the red waveband is absorbed at a higher rate by the water column than blue or green wavebands.

c. Effect of Surface Waves

Both methods are affected by the water surface and the noise created by variable reflection of light from waves and ripples. The sea surface correction algorithm goes a long way to reduce these effects, but does not eliminate them. Figure 24 shows the variability of reflection from the sea surface caused by surface ripples, the right hand image is taken with the NIR band and gives radiance values for the top most layer of the water column. The NIR image is compared with the true colour image, of the same area on the left, to highlight how to a lesser effect the visible wavebands are influenced by variable surface reflection. Figure 25 gives the Digital Number (DN) values received at the satellite for the NIR image and shows the amount of noise caused by sea surface ripples. It is assumed that a similar pattern at lower amplitude is present in the red, green

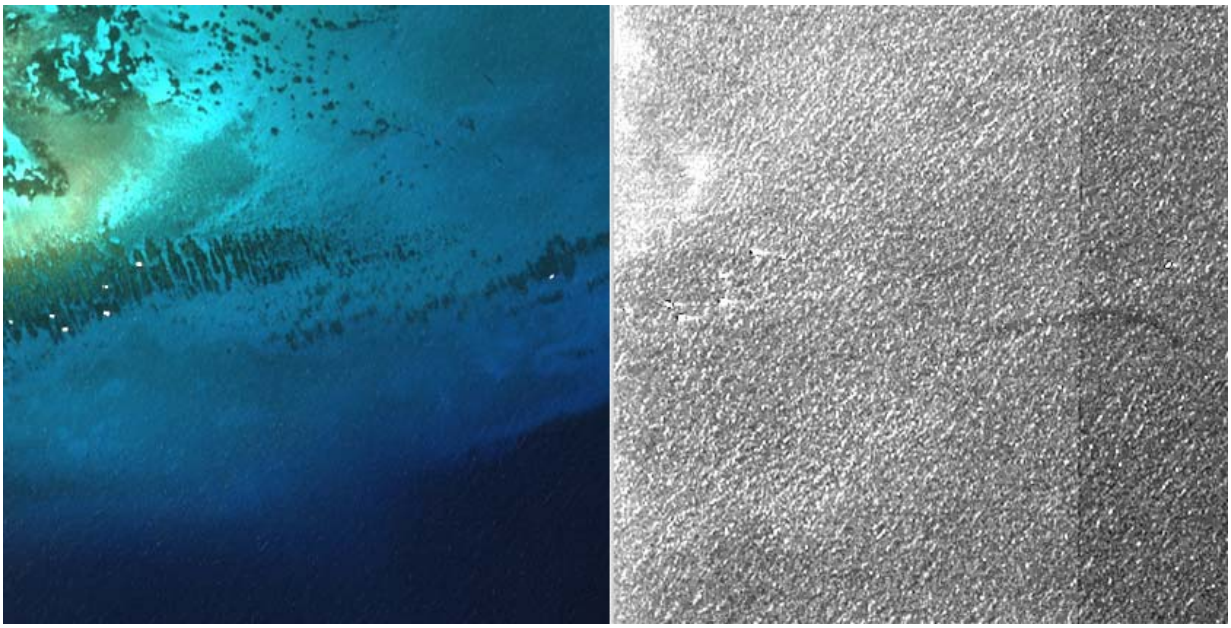

Figure 24. True colour and NIR images from the same image and area of Looe Key highlighting surface ripple effects on radiance values received at the satellite.

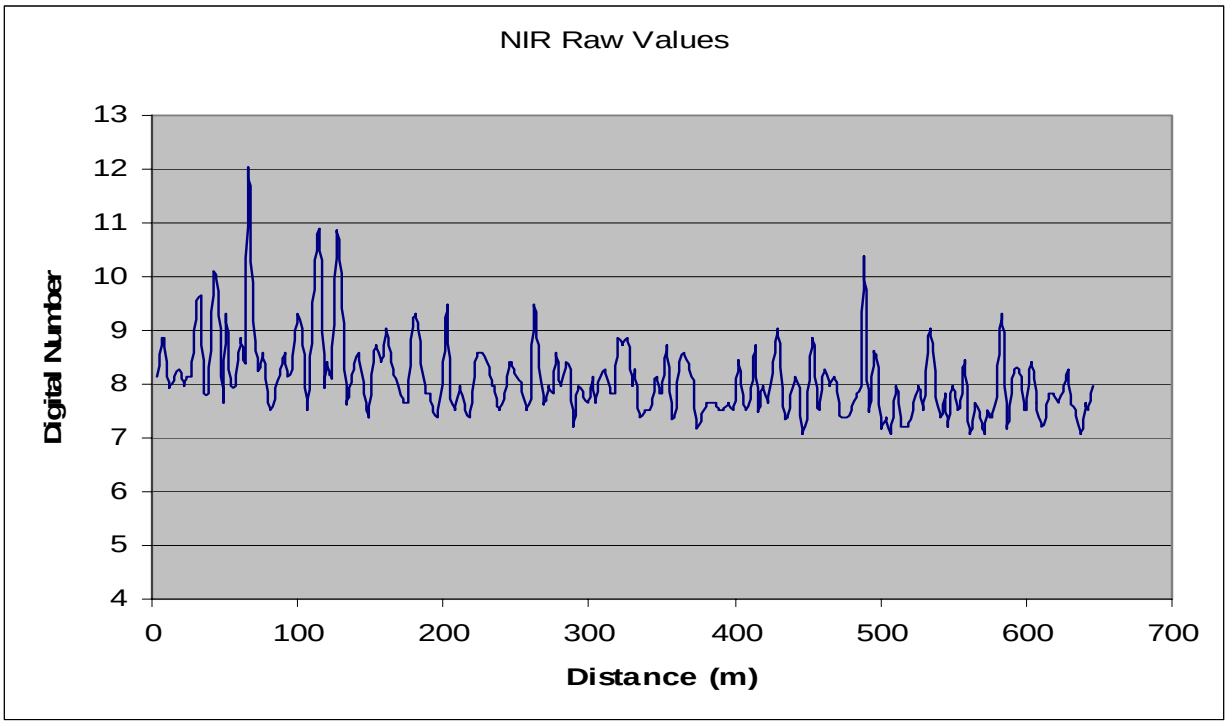

Figure 25. NIR DN values for the Looe Key transect highlighting the variability of the received signal caused by surface ripple effects.

and blue wavebands that create a sinusoidal pattern in the two algorithms when calculating water depth.

d. Effect of Non-Homogenous Water

Remote sensing methods rely on the target area having a homogenous body of water, both horizontally and vertically. In the case of Plymouth Sound a band of run-off crosses the transect with greater amounts of silt and particulate matter. The algorithm underestimates depths in the run-off because the increased sediment gives the water column a lighter colour, which is miss-read to be shallower than the charted depths.

D. DEPTH IMAGE OUTPUT

The ENVI output images for both areas are shown in Figs 26 and 27. These bathymetry graphics agree with the chart data for each area and provide a greater degree of detail than a standard nautical chart. Small bathymetric changes, due to shifting sands and silts for example, can be readily determined through the use of satellite imagery and exported in a variety of formats.

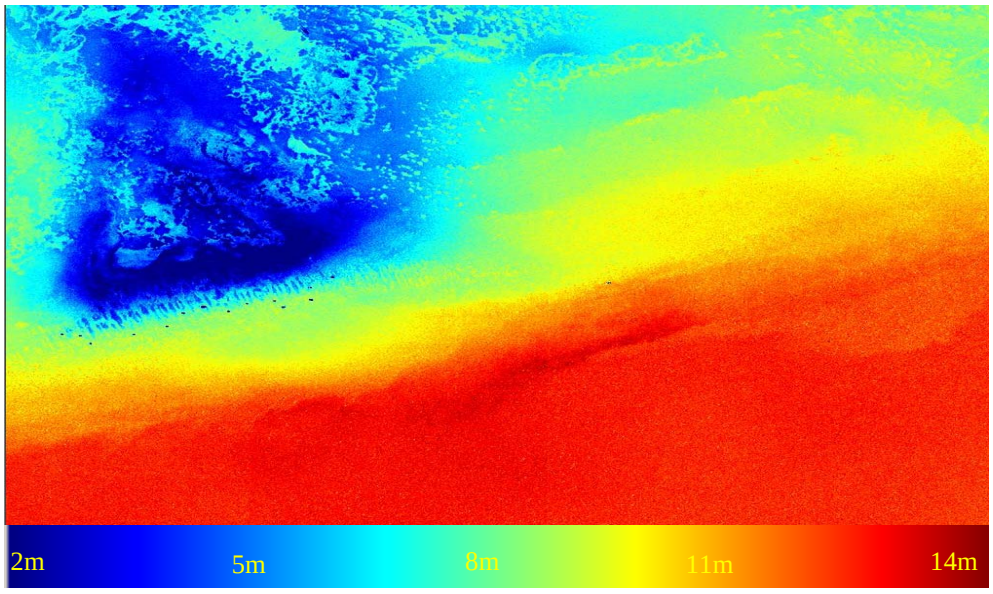

Figure 26. QB derived bathymetry for Looe Key using the ratio algorithm.

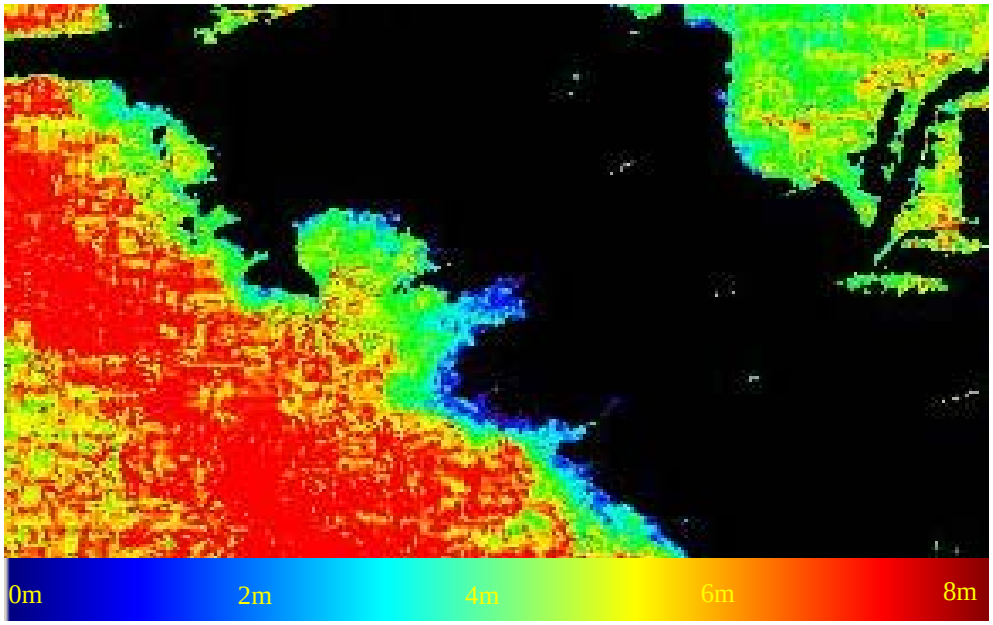

Figure 27. QB derived bathymetry for Plymouth Sound using the turbidity algorithm.

VI. CONCLUSION AND RECOMMENDATIONS

A. CONCLUSIONS

This study uses multi-spectral QuickBird imagery with a nominal resolution of 2.6m to derive seabed bathymetry at two separate locations, Looe Key (USA) and Plymouth Sound (UK). A series of corrections for the atmosphere, the sea surface and the water column are employed to convert the blue, green and red wavebands to reflectance values. The NPS AOD algorithm, a sea surface glint correction algorithm and HYDROLIGHT modeling, is used to determine the corrections required, and the resultant reflectance values are incorporated into a ratio (clear water) and turbidity (estuarine water) algorithm to derive water depth. The Looe Key results are compared to LIDAR bathymetry obtained in 2004 and the Plymouth Sound results compared to hydrographic survey data collected between 1963-72.

The results show that the standard ratio and turbidity algorithms provide an accurate representation of seabed bathymetry in the clear water of Looe Key, with average errors of 11.7% and 16.5% respectively. In the turbid water of Plymouth Sound, the error of the turbidity algorithm averages 11.6%. Although the standard ratio algorithm was found not to return valid results at Plymouth, an amended version returned results with an average error of 13%.

The accuracy of QuickBird derived bathymetry does not meet the requirements of the International Hydrographic Office's minimum standards for depth uncertainties for inshore waters. However, the low average error of these algorithms, in clear and turbid waters, suggests that these methods offer significant potential for determining shallow water bathymetry in the littoral zone.

B. RECOMMENDATIONS

The performance of both algorithms is dependant on four main environmental factors. To improve the accuracy of satellite-derived bathymetry, the following recommendations are proposed:

1. Resolve Variable Bottom Type

Variable bottom types in an image should be masked and analysed individually to avoid spikes like that over the coral fingers at Looe Key. The target image should be separated into areas of similar bottom type and reflection coefficients derived for each area to be incorporated into a depth algorithm.

2. Resolve Light Attenuation

The extent to which light attenuates in water restricts the depth to which an algorithm operates. In turbid water, the QB red and green wavebands are more prone to absorption, and therefore, are limited in the depth to which they can retrieve accurate depth estimates. Similar depth analyses in turbid water with different sensors that have different red and green waveband sensors may provide greater depth penetration than those of QB.

3. Resolve Surface Effects

An analysis of surface waves and ripples could be used to determine a sinusoidal wave pattern in the derived depth profile. If this was subtracted from the depth profile, or a dedicated sampling procedure developed, the noise could be corrected for.

4. Resolve Non-Homogeneous Water

An analysis to determine the horizontal variability of matter in the water column, such as the chlorophyll method developed in this study, would give more accurate water coefficient results when modeled in software such as HYDROLIGHT. The results when incorporated into HYDROLIGHT as individual pixel values would give attenuation coefficient values for each pixel. Such values will enable an algorithm to analyse an area of non-homogeneous water more accurately.

LIST OF REFERENCES

Bierwith, P. N., Lee, T., Burne, R. V., 1992: Shallow sea-floor reflectance and water depth derived by unmixing multispectral imagery. *First Thematic Conference on Remote Sensing for Marine and Coastal Environments.*

Brown, B. B., 1997: Remote measurement of aerosol optical properties using the NOAA POES AVHRR and GOES imager during TARFOX. Master's Thesis, Naval Postgraduate School, Monterey, California.

Durkee, P. A., D. R., Jensen, E. E., Hindman, T. H., Vonder Haar., 1986: The relationship between marine aerosol particles and satellite-derived radiance. *Journal of Geophysical Research*., 91, 4063-4072.

Durkee, P. A., Pfiel, F., Frost, E., Shema, R., 1991: Global analysis of aerosol particle characteristics. *Atmospheric Environment*., 25(A), 2457-2471.

Clark, R. E., 2005: Naval satellite bathymetry: A performance assessment. Master's Thesis, Naval Postgraduate School, Monterey, California.

Fisher, T. M., 1999: Shallow water bathymetry at Lake Tahoe from AVIRIS Data Master's Thesis, Naval Postgraduate School, Monterey, California.

Gordon, R. H., Clark, D. K., 1981: Clear water radiances for atmospheric correction of coastal zone color scanner imagery. *Applied Optics*, 24, 4175-4180.

Gianinetto, M. and Lechi, G., 2003: A DNA algorithm for the bathymetric mapping of the lagoon of Venice using QuickBird multispectral data.

Hochberg, E. J., Andrefouet, S., Tyler M. R., 2003: Sea surface correction of high spatial resolution ikonos images to improve bottom mapping in near-shore environments. *IEEE Transactions on Geoscience and Remote Sensing*, 1724-1729.

Jerlov, N. G., 1976: *Marine Optics*, Elsevier, Amsterdam.

Jupp, D. L. B., 1988: Background and extensions to depth of penetration (DOP) mapping in shallow coastal waters. *Symposium on Remote Sensing of the Coastal Zone*.

Lafon, V., Froidefond, J. M., Lahet, F., Castaing, P., 2002: SPOT shallow water bathymetry of a moderately turbid tidal inlet based on field measurements. *Remore Sensing of Environment*, 136-148.

Lavender, S., Nagur Cherukuru, R. C., Doxaran, D., 2004: High spatial resolution remote sensing of the Plymouth coastal waters. *Proceedings of 2nd* CHRIS/*Proba Workshop, ESA/ESRN, Frascati, Italy*.

Lyzenga, D. R., 1978: Passive remote sensing techniques for mapping water depth and bottom features. *Applied Optics*, 379-383.

Lyzenga, D. R., 1981: Remote sensing of bottom reflectance and water attenuation parameters in shallow water using aircraft and Landsat data. *International Journal of Remote Sensing*, 71-82.

Lyzenga, D. R., 1985: Shallow-water bathymetry using combined lidar and passive multispectral scanner data. *International Journal of Remote Sensing*, 115-125.

Martin, J.S., 2004: Aerosol opitcal depth model assessment with high resolution multiple angle sensors. Master's Thesis, Naval Postgraduate School, Monterey, California.

Melsheimer, C. and Liew, S. C., 2001: Extracting bathymetry from multi-temporal SPOT images. *22nd Asian Conference on Remote Sensing*.

Mobley, C. D., 1995: *HYDROLIGHT 3.0 Users' Guide*. SRI International, Menlo Park, California.

Philpot, W. D., 1989: Bathymetric mapping with passive multispectral imagery. *Applied Optics*, 1569-1578.

Stumpf, R. P., Holderied K., Robinson, J. A., Feldman, G., Kuring, N., 2003: Mapping water depths in clear water from space. *Proceedings of the 13th Biennial Coastal Zone Conference*.

Stumpf, R. P., Holderied K., Sinclair, M., 2002: Mapping coral reef bathymetry with high-resolution, multispectral satellite imagery. *Seventh International Conference on Remote Sensing for Marine and Coastal Environments*.

Tanis, F. J., Malinas, N. P., Arbor, A, Holland, D., Albasini, J., 2002: Shallow water extraction algorithm for bathymetry and bottom features. *Seventh International Conference on Remote Sensing for Marine and Coastal Environments*.

INITIAL DISTRIBUTION LIST

1. Defense Technical Information Center
   Ft. Belvoir, Virginia

2. Dudley Knox Library
   Naval Postgraduate School
   Monterey, California

3. Professor Mary L. Batteen
   Department of Meteorology
   Naval Postgraduate School
   Monterey, California

4. Professor Philip A. Durkee
   Department of Meteorology
   Naval Postgraduate School
   Monterey, California

5. Professor Edward Thornton
   Department of Meteorology
   Naval Postgraduate School
   Monterey, California

6. Captain Simon Bevan Royal Navy
   DIJE
   Main Building
   Whitehall
   London SW1A 2HB
   United Kingdom

7. Commander Peter Greenwood Royal Navy
   British Embassy
   Washington DC 20008

8. Lieutenant Commander Steve Hipsey Royal Navy
   HMTG
   HMNB Devonport
   Plymouth
   Devon PL2 2BG
   United Kingdom

9. Lieutenant Martin Densham Royal Navy
FNMOC
7 Grace Hopper Avenue
Monterey
California CA93943